ACCSCIENCE PUBLISHING

International Journal of Bioprinting

RESEARCH ARTICLE

A pilot evaluation of a 3D bioprinted tumor model for assessment of electroporation-based therapies

Franca Scocozza[1], Silvia Pisani[2,3,*], Aleksandra Evangelista[3], Ferdinando Auricchio[1], Michele Conti[1,5], Bice Conti[2,3] and Marco Benazzo[3,4]

[1] Department of Civil Engineering and Architecture, Faculty of Engineering, University of Pavia, Pavia, Italy

[2] Department of Drug Sciences, University of Pavia, Pavia, Italy

[3] Department of Otorhinolaryngology, IRCCS Polyclinic San Matteo Foundation, Pavia, Italy

[4] Department of Clinical-Surgical, Diagnostic, And Pediatric Sciences - Integrated Unit Of Experimental Surgery, Advanced Microsurgery, And Regenerative Medicine, University of Pavia, Italy

[5] Computer Simulation Laboratory, IRCCS Polyclinic San Donato, Milan, Italy

(This article belongs to the *Special Issue*: *Advanced Strategies in 3D Bioprinting for Disease Modelling*)

Abstract

Head and neck squamous cell carcinomas (HNSCCs) are aggressive malignancies with poor prognosis and limited therapeutic options. Electrochemotherapy (ECT), combining short electric pulses with chemotherapeutic agents to enhance intracellular drug uptake, has shown clinical potential but still requires physiologically relevant *in vitro* models for protocol optimization and mechanistic studies. Here, we introduce a three-dimensional 3D bioprinted *in vitro* HNSCC model specifically designed for the assessment of electroporation. Structures were fabricated using a composite hydrogel composed of 8% sodium alginate and 4% gelatin (w/w), crosslinked with calcium chloride at concentrations of 0.5%, 1%, and 2%. Uniaxial compression testing confirmed elastic moduli spanning the physiological tumor stiffness range, with the 1% calcium chloride formulation providing optimal mechanical and handling characteristics (42.96 ± 19.89 kPa). Hypopharyngeal carcinoma FaDu cells (5×10^6/mL) embedded in three-layer structures (thickness: 1.05 mm) maintained 75–80% viability for up to 21 days and formed tumor-like spheroids (mean diameter: 303 ± 113 µm), reflecting native tumor architecture. Electroporation with eight pulses at 200 V for 100 µs efficiently permeabilized the cell membrane, as evidenced by the internalization of propidium iodide, while maintaining high cell viability as confirmed by live/dead analysis. Programmed death-ligand 1 expression was preserved and upregulated in 3D spheroids compared to two-dimensional (2D) controls, supporting the platform's relevance for immuno-oncology studies. Compared to other 3D HNSCC models, our system integrates mechanical tuning, electroporation compatibility, and immune-related biomarker expression, enabling functional validation of electric field-mediated intracellular delivery. This proof-of-concept platform demonstrates structural fidelity, long-term cell viability, and high reproducibility, offering a scalable, human-relevant tool for preclinical optimization of ECT and other electrically based therapies, bridging the gap between conventional 2D cultures and complex *in vivo* models.

***Corresponding author:**
Silvia Pisani
(silvia.pisani@unipv.it)

Citation: Scocozza F, Pisani S, Evangelista A, *et al.* A pilot evaluation of a 3D bioprinted tumor model for assessment of electroporation-based therapies. *Int J Bioprint*. 2026:12(2):025430434.
doi: 10.36922/IJB025430434

Received: October 21, 2025
Revised: November 28, 2025
Accepted: December 3, 2025
Published online: December 3, 2025

Keywords: Bioprinting; Electroporation; FaDu cancer cells; Head and neck cancer; Three-dimensional cancer model.

1. Introduction

Head and neck squamous cell carcinomas (HNSCCs) are clinically challenging due to aggressive behavior, complex anatomy, and limited treatment options, arising mainly from the mucosal epithelium of the oral cavity, pharynx, and larynx.[1] Their high metastatic potential and poor prognosis underscore the need for improved localized therapies.[2] Current treatments—surgery, radiotherapy, and chemotherapy—are often limited by tumor location, collateral damage, and systemic toxicity.[3-5]

Electrochemotherapy (ECT) offers a promising alternative by combining short, high-intensity electrical pulses (electroporation) with drug administration, thereby enhancing cancer cell membrane permeability and drug uptake.[6,7] The transient formation of hydrophilic pores allows the entry of therapeutic molecules without permanently compromising tumor cell viability. Clinically, ECT is widely applied to skin metastases and tumors unsuitable for surgery, following European standard protocols (European Standard Operating Procedures of Electrochemotherapy [ESOPE]).[8,9] For HNSCC, bleomycin is commonly used with eight 100-µs pulses at 1 kV/cm and 5 kHz.[10] Despite encouraging results, ECT still faces challenges, including variable treatment responses, precise electrode placement requirements, and reduced efficacy in poorly vascularized tumors.[11] These limitations underscore the need for reliable and physiologically relevant preclinical models that accurately reproduce tumor biology and electrical properties, thereby supporting the optimization of electric field parameters, drug combinations, and the mechanistic understanding of electroporation.

In vivo models remain the gold standard but are costly, ethically challenging, and often poorly predictive due to interspecies differences. Conversely, two-dimensional (2D) cultures fail to reproduce the complex tumor microenvironment. Advanced three-dimensional (3D) systems, such as organoids and organ-on-chip models, improve physiological relevance but offer limited control over geometry, mechanical properties, and electrode configuration, reducing their suitability for electroporation studies.

Head and neck squamous cell carcinomas present additional modeling challenges due to their anatomical location, stromal complexity, extracellular matrix (ECM) heterogeneity, and distinct bioelectric features that influence treatment response. Effective models must therefore recapitulate ECM architecture, stromal interactions, nutrient/oxygen gradients, and electromechanical heterogeneities.

Three-dimensional bioprinting addresses many of these limitations by enabling spatially defined architectures with controlled composition and stiffness, supporting standardized and reproducible tumor models.[12,13] Recent reviews highlight its potential to reconstruct HNSCC microenvironments with improved physiological relevance and tunable mechanical and bioelectrical properties.[14,15] Advances such as multi-material extrusion, coaxial printing, droplet-based systems, and volumetric bioprinting further enhance micro- and macroenvironmental control.[16,17] Among these approaches, extrusion-based bioprinting remains widely used for tumor models due to its simplicity, versatility, and ability to generate reproducible structures.

Existing bioprinted HNSCC models—including hydrogel structures[18] and nanocellulose-based bioinks for radiochemotherapy testing[19] —successfully generate viable spheroids but rarely incorporate electroporation-specific parameters such as electrical conductivity, dielectric properties, or optimized electrode geometries. Most systems focus on recapitulating tumor architecture or supporting drug screening, typically embedding immortalized cell lines in hydrogels such as alginate, gelatin (GEL), or decellularized ECM to form reproducible, viable spheroids. For example, Kort-Mascort *et al.*[18] reported alginate–GEL structures supplemented with decellularized porcine tongue ECM, where UM-SCC-12 or UM-SCC-38 cells formed spheroids over 2–3 weeks; a subsequent study incorporating fibroblasts (A8-HVFFs) reproduced tumor–stroma organization, with cancer cells in the core and fibroblasts at the periphery.[18,20] These studies demonstrate the reproducibility and biological relevance of bioprinted HNSCC models for drug testing; however, they still lack the integration of electroporation-relevant parameters, such as electrical conductivity and dielectric behavior.

The present study addresses this gap by developing and characterizing a pilot 3D bioprinted HNSCC model specifically designed for electroporation applications. The model integrates key mechanical and biological features of tumor tissue, supports long-term cell viability, and enables controlled application of electric fields. This proof-

of-concept platform provides a basis for improving ECT protocols and reducing reliance on *in vivo* and extensive preclinical testing.

2. Materials and methods

In this study, we established a 3D bioprinted HNSCC tumor model using a pneumatic extrusion-based approach. The workflow involves incorporating HNSCC cells into a sodium alginate (SA)–GEL hydrogel, followed by the deposition of the bioink according to a predefined computer-aided design geometry and subsequent ionic crosslinking. Figure 1 provides a schematic overview of the entire process, including bioink preparation, printing steps, and post-print crosslinking of the fabricated construct.

2.1. Biomaterial ink formulation and crosslinking

We selected an SA–GEL bioink for its mechanical compatibility with tumor tissue and electrical properties relevant to electroporation. SA–GEL has been successfully used in 3D bioprinted HNSCC models, supporting spheroid formation and high cell viability.[20] We also previously applied SA–GEL in a 3D osteosarcoma model, where cell and tissue elastic moduli were comparable to those of HNSCC (0.5–7.5 kPa for osteosarcoma cells; 10–100 kPa for non-mineralized tumor tissue),[21-23] justifying its use to approximate tumor stiffness *in vitro*. Additionally, crosslinking SA–GEL with calcium ions generates an ionically conductive matrix, supporting electric field penetration during electroporation.[24,25] Although these electrical properties were not directly measured in this study, the composition and crosslinking conditions were chosen based on literature and prior experience to ensure a conductive environment compatible with microsecond pulse delivery and cell viability.[26-28]

Briefly, the biomaterial ink was prepared by dissolving the GEL powder in sterile phosphate-buffered saline (EuroClone, Italy), which had been preheated to 72°C. SA powder was then added to the GEL solution and vortexed until a homogeneous mixture was achieved. The mixture was centrifuged (2,000 rpm, five minutes) to remove air bubbles and pasteurized in a water bath at 72°C for one hour. The final concentrations of the hydrogel were 8% wt SA and 4% wt GEL. The hydrogel was stored in sterile syringes at 4°C until further use.

Crosslinking was performed by immersing the hydrogel in calcium chloride ($CaCl_2$) solutions prepared in deionized water at room temperature. To optimize both mechanical integrity and ionic conductivity, different $CaCl_2$ concentrations (0.5%, 1%, & 2% wt) were tested. Additionally, considering subsequent cell embedding, the osmolarity of the crosslinking solutions was estimated to ensure compatibility with cell viability. The osmolarity was calculated using **Equation (1)**:

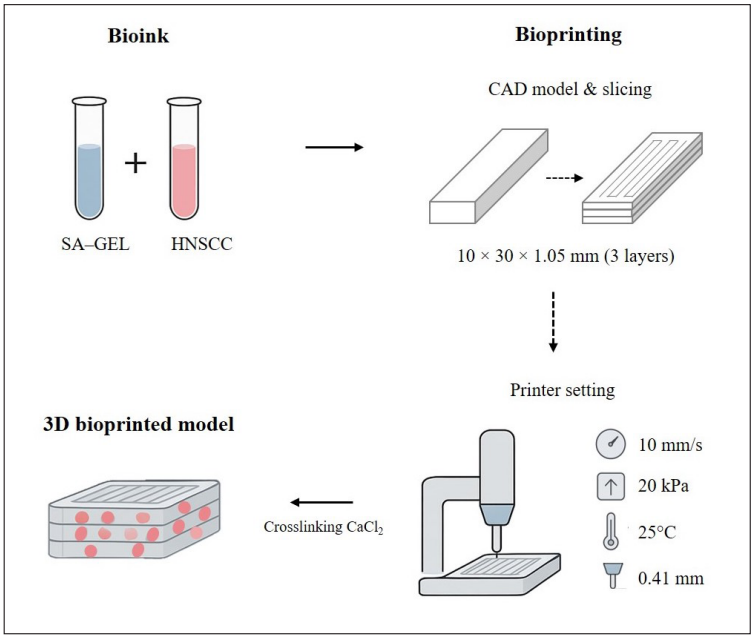

Figure 1. The stepwise process used to fabricate the three-dimensional (3D) head and neck squamous cell carcinoma (HNSCC) model. HNSCC cells were incorporated into a sodium alginate (SA)–gelatin (GEL) bioink, digitally modeled using a predefined computer-aided design (CAD), and printed via pneumatic extrusion under optimized parameters. The printed construct was subsequently subjected to calcium chloride ($CaCl_2$)-mediated ionic crosslinking to obtain the final stabilized hydrogel structure.

$$O = n \times C \quad (1)$$

where n represents the number of particles (molecules or ions) into which one formula unit of solute dissociates, and C is the molar concentration of the solute (mol/L). Once printed, the structures were crosslinked by immersion in 5 mL of $CaCl_2$ solution (0.5%, 1%, & 2% wt) for seven minutes. This ionic crosslinking stabilized the structures, enhanced mechanical integrity, and maintained conductivity compatible with electroporation, while preserving 3D architecture and handling robustness for subsequent electroporation treatment. All reagents were obtained from Sigma-Aldrich (Italy).

2.2. Mechanical characterization of biomaterial ink

Mechanical characterization was performed to match the hydrogel stiffness with that of native tumor tissue, which typically ranges from 10–38 kPa in HNSCC.[29-31] Hydrogel stiffness was adjusted by varying $CaCl_2$ concentration during crosslinking. Uniaxial compression tests were conducted as previously describe.[32] Cylindrical specimens with a diameter of 8 mm and a height of 6 mm were prepared. The samples were made using 3D-printed molds. Each mold was placed inside a Petri dish, and the hydrogel was dispensed into it using a syringe. The samples were immersed in a $CaCl_2$ solution for one hour to ensure that the solution reached the entire structure. The influence of $CaCl_2$ concentration was evaluated by considering three different $CaCl_2$ concentrations: 0.5%, 1% and 2% (wt). Multiple batches were prepared at different times to assess the repeatability of the preparation process. All analyses were performed in triplicate (n = 3 independent batches, each containing 10 specimens, for a total of n = 30).

An MTS Insight Electromechanical Testing System (MTS System Corporation, United States) with a 250 N load cell was used for the mechanical test. The preload was set at 0.03 N, representing a minimal force sufficient to ensure that the sample was fully in contact with the upper plate before the test commenced. The test speed was 0.2 mm/min. Samples were compressed until failure at room temperature (22–24°C), while force and displacement were recorded simultaneously.

After compression, the data were processed. Force–displacement data, from the preload threshold to the failure point, were used for analysis. Nominal stress (σ) was calculated as the applied force divided by the sample's cross-sectional area ($\sigma = F / A$), and strain (ε) as the displacement normalized to the sample's initial height ($\varepsilon = \Delta L / L_0$). Only the linear region of the stress–strain curve, corresponding to strains up to 15%, was considered. A spline approximation was used to evaluate local stiffness by computing its first derivative, and the maximum derivative value within the selected strain range was taken as the elastic modulus (E). The mean value of E was then calculated.

2.3. 3D bioprinted head and neck squamous cell carcinoma model for electroporation

A 3D *in vitro* model of HNSCC was developed using direct extrusion-based bioprinting for electroporation experiments. Electroporation was performed using the Genedrive device (IGEA Medical, Italy).[8] This device utilizes adaptive electroporation technology, specifically tailored for preclinical studies, allowing users to customize the electric pulse amplitude, frequency, duration, and waveform. We used cuvettes to apply the targeted electrical pulses (Figure 2A). The bioprinted model was placed in the cuvette with a 2 mm gap width, which would subsequently be positioned within the electroporation device. To this end, a computer-aided design model of a parallelepiped-shaped structure with dimensions of 30 × 10 mm was designed. The structure thickness was optimized (1.05–1.3 mm) to account for the cuvette gap and ensure efficient current passage.

Bioprinting was performed with the CELLINK BioX-Gen 3 (CELLINK AB, Sweden). The bioprinter is designed to facilitate cleaning and maintain sterility, which is critical for cell-based applications. It provides a sterile printing environment, reducing the risk of contamination when working with cells. The computer-aided design model was sliced with a layer height of 0.35 mm and 75% infill to generate a solid structure without internal porosity. SA–GEL ink was loaded into a cartridge, briefly centrifuged (≤1,000 rpm), and printed at 10 mm/s and 20 kPa at room temperature. After printing, the structures were crosslinked in CaCl2 for seven minutes. Full parameters are reported in Table 1. Figure 2B shows the printed structure. All printing and crosslinking operations were performed at room temperature.

For electroporation, structures were positioned vertically in the cuvette (Figure 2C). The electroporation parameters—pulse duration, amplitude, and frequency—were selected in accordance with the ESOPE clinical protocols for head and neck ECT.[8] The parameters used in this study followed the ESOPE clinical electroporation guidelines, which recommend an electric field strength of 1,000 V/cm, a pulse duration of 100 µs, a 20 µs interpulse interval, and eight pulses.[6,9] Given that the gap of our electroporation cuvette was 2 mm (0.2 cm), the voltage required to achieve the ESOPE-recommended field strength was 200 V. Thus, applying 200 V corresponds to the ESOPE protocol conditions for generating the appropriate electric field magnitude within our construct. To ensure

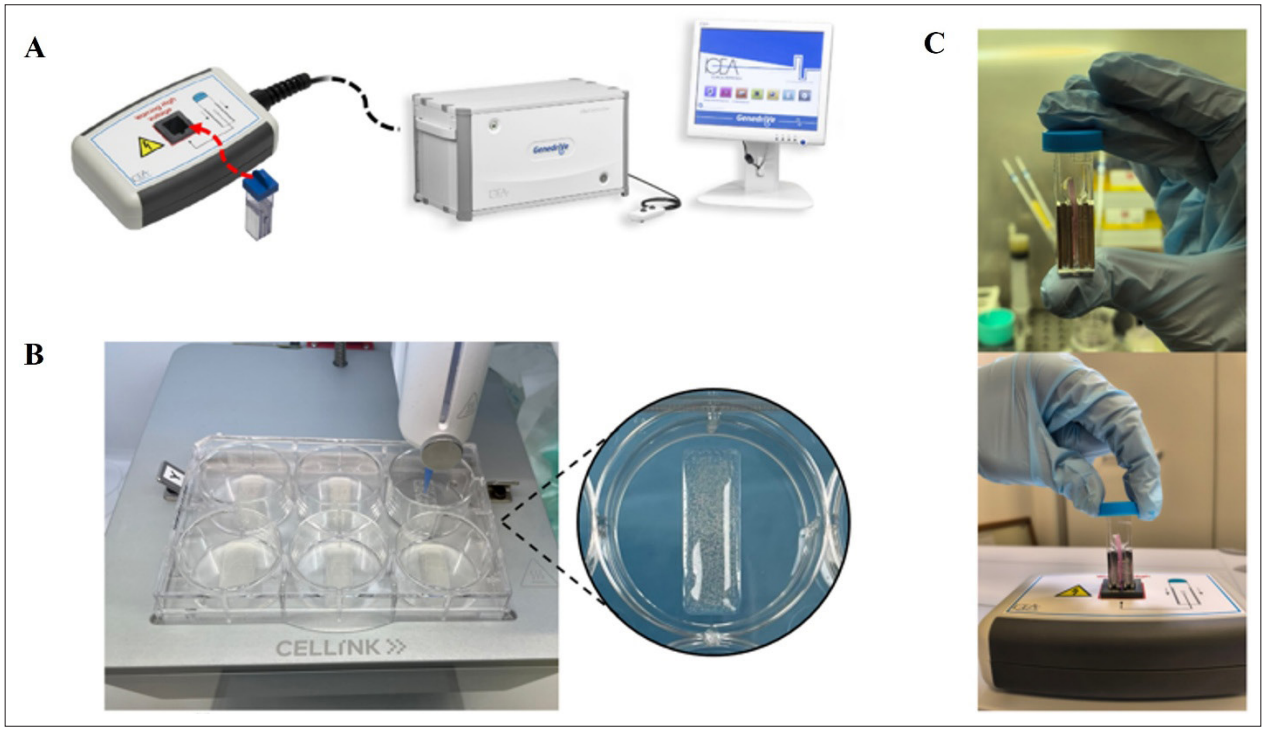

Figure 2. Electroporation of a three-dimensional (3D) bioprinted head and neck model. (A) Igea Medical Electroporation Genedrive device. (B) 3D bioprinted structures were placed into 6-well plates. (C) The printed structures were placed into the cuvettes using sterile tweezers and electroporated.

Table 1. Bioprinting parameters, ranges tested, and optimized values

Bioprinting parameter	Range tested	Optimized value
Number of layers	3–4	3
Infill density	65–85%	75%
Infill pattern	Rectilinear/Concentric	Rectilinear
Printing speed	5–15 mm/s	10 mm/s
Printing pressure	8–22 kPa	20 kPa
Print-head temperature	Room temperature–30°C	25°C
Print-bed temperature	Room temperature–30°C	Room temperature
Nozzle inner diameter	0.41 mm	0.41 mm
Crosslinking concentration	0.5–2% wt calcium chloride	1% wt calcium chloride

a robust operating range and verify that the hydrogel structure could tolerate a slightly higher field without detrimental effects, we additionally included experiments at 300 V. This higher voltage condition provided a safety margin, confirming that effective electroporation can still occur under slightly more demanding conditions while remaining within widely used and safe electroporation parameters. Both three-layer (3L) and four-layer (4L) structures were tested to evaluate the effects of thickness on current distribution and structural stability. The complete electroporation settings are listed in Table 2.

2.4. Morphological characterization of 3D bioprinted structure

The uniformity of the bioprinted structure was evaluated through detailed morphological characterization using scanning electron microscopy (SEM; Zeiss EVO MA10, Carl Zeiss, Germany). Before SEM analysis, the structures underwent a freeze-drying process (lyophilization) to

Table 2. Genedrive electroporator parameters used for electroporation of sodium alginate–gelatin bioprinted gels

Electroporation parameters	Set values
Pulse number	8
Pulse duration	100 μs
Interpulse interval	20 μs
Voltage	200 V or 300 V

preserve their 3D architecture and prevent structural collapse during imaging. Specifically, samples were frozen and dehydrated under controlled conditions at −50°C and 0.2 mbar using a freeze dryer (Epsilon 2-4 LSCplus, Infitek Co., Ltd., China). Following lyophilization, the dried structures were weighed using an analytical balance (Entris, Sartorius AG, Germany) to confirm mass uniformity across replicates, thereby indirectly verifying the reproducibility of the printing process.

For SEM preparation, lyophilized structures were carefully mounted on aluminum stubs with conductive carbon tape to ensure sample stability and minimize charging effects. To further enhance surface conductivity and improve image resolution, the samples were sputter-coated with an ultrathin layer of gold (~10 nm) using a precision sputter coater. This conductive coating allowed high-quality SEM imaging, enabling detailed visualization of surface topography, pore distribution, and overall morphological features of the bioprinted structures. Image processing was performed through grayscale conversion and Gaussian filtering ($\sigma = 1$) to suppress high-frequency noise. Pores were segmented using a modified Otsu threshold (scaled by 0.70), and the resulting binary mask was inverted so that pores appeared as white regions. Porosity was calculated as the percentage of white pixels relative to the total image area, after eliminating particles smaller than 50 pixels.[2] The pixel-to-micrometer conversion was obtained through manual measurement of the 10 μm scale bar. Validation was performed by: (i) testing the pipeline on SEM images from different samples and magnifications to confirm parameter robustness; (ii) repeating the manual calibration with two independent operators (variation <3%); and (iii) comparing porosity outputs across technical replicates, which showed low variability (43.8 ± 5.9%). A code excerpt has been added to the **Supplementary File**.

2.5. FaDu cell incorporation in 3D bioprinted structures

Hypopharyngeal carcinoma (FaDu) cells (HTB-43TM, American Type Culture Collection, United States) were selected for their programmed death-ligand 1 (PD-L1) positivity, making them relevant for studies of tumor-immune interactions and programmed death-1/PD-L1-targeted therapies.[33] They are also widely used in subcutaneous xenograft models due to their ability to form tumors, enabling assessment of tumor growth, treatment response, and microenvironment interactions.[34,35]

Cells were cultured in DMEM-GlutaMAX supplemented with 10% fetal bovine serum and 1% penicillin–streptomycin at 37°C and 5% carbon dioxide. Medium was replaced every 2–3 days, and confluence was monitored to maintain healthy proliferation. Cells at or below passage 5 were detached with trypsin-ethylenediaminetetraacetic acid, counted, and assessed for viability via trypan blue. All procedures were performed under sterile conditions in a laminar flow hood.

For bioprinting, the cells were gently mixed with the SA–GEL ink (5×10^6 cells/mL) using two syringes connected by a Luer lock at a 1:10 (cell suspension:hydrogel) volume ratio to form the bioink. The bioink was then loaded into a cartridge and subjected to short-run centrifugation to remove air bubbles and compact the mixture. The cartridge was connected to a needle nozzle and placed in a bioprinter. Before printing, the BioX automatic ultraviolet sterilization cycle (365 nm) was performed. Structures were bioprinted in 6-well plates (Figure 2B) according to the process described in **Section 2.3**. After printing, each structure was crosslinked by immersion in the selected $CaCl_2$ solution for seven minutes. The $CaCl_2$ solution was then removed, and 5 mL of cell culture medium was added.

For electroporation, structures were placed in cuvettes using sterile tweezers and treated as described in Table 2 (Figure 2C). After electroporation, the structures were returned to fresh medium and incubated at 37°C with 5% carbon dioxide for up to 21 days.

2.6. Live/dead and cluster analysis in 3D bioprinted head and neck squamous cell carcinoma models

For the live/dead assay and cluster analysis, a total of 18 structures were bioprinted (nine without electroporation and nine with electroporation). FaDu cell viability and proliferation at 7, 14, and 21 days ($n = 3$ samples per time point) were assessed using the Live/Dead kit (L3224, Invitrogen™, Thermo Fisher Scientific Inc., United States). Samples were incubated with the dye for 10 minutes, rinsed with distilled water to remove excess dye, and analyzed using an immunofluorescence microscope (Leica DM IL, LED-FLUO, Leica Microsystems Srl, Italy). Images were processed in Fiji/ImageJ (version 1.54r), and the percentage of live cells was calculated using **Equation (2)**:

$$\% \text{ Live cells} = [\text{Live cells}/(\text{Live cells} + \text{dead cells})] \times 100 \quad (2)$$

Means and standard deviations (n = 3) were reported. 4',6-diamidino-2-phenylindole (DAPI) staining (Invitrogen™, Thermo Fisher Scientific Inc., United States) at 1 μg/mL in sterile phosphate-buffered saline was used to visualize cell nuclei.

The selected time points (7, 14, & 21 days) were chosen to monitor cell viability across the key phases of hydrogel maturation and tumor-like cluster development. In 3D constructs, cells typically undergo an initial adaptation period (first week), followed by progressive cluster formation and ECM remodeling (second week), and establishment of mature, densely populated aggregates by day 21. These time points, therefore, capture the temporal evolution of cell survival and 3D organization within the hydrogel, allowing us to assess both the short-term and long-term effects of electroporation on cell viability.[21,32,36]

Tumor cell cluster formation was assessed both qualitatively and quantitatively using Fiji/ImageJ, employing standard thresholding and particle analysis workflows that were applied consistently across all samples. Both live/dead and cluster analyses were performed in duplicate.

2.7. Propidium iodide uptake in 3D bioprinted structure under electroporation

The SA–GEL hydrogel was tested for its ability to permit the passage of a hydrophilic model molecule across cell membranes under electroporation using propidium iodide (PI; Thermo Fisher Scientific Inc., United States). PI is commonly used in ECT studies because it mimics the limited membrane permeability of anticancer drugs, intercalates into DNA, and allows direct fluorescence-based monitoring of uptake and localization.[37] It exhibits maximum excitation at 535 nm and emission at 617 nm, making it compatible with other fluorophores. Studies in Chinese hamster ovary cells have shown that PI uptake depends predictably on electric field strength, validating theoretical models and emphasizing the importance of precise field calibration.[38,39]

For PI uptake assessment, a total of 12 structures were bioprinted (six without electroporation and six with electroporation). After 14 and 21 days of incubation (n = 3 samples per time point), based on cell viability and cluster formation, a 50 μM PI solution in 1% wt $CaCl_2$ was injected (200 μL per structure) using a 30 G needle. Six injection points were applied per structure to simulate intratumoral delivery and minimize local concentration gradients by distributing the dye throughout the construct volume. The injection sites were positioned symmetrically along the longitudinal axis of the construct, and the delay between injection and electroporation was kept constant for all samples, so that any residual heterogeneity in PI concentration was comparable across experiments. PI uptake was quantified as the average fluorescence intensity over the entire construct, thereby averaging out potential local differences relative to the injection sites and electrode surfaces. The six electroporation structures were then placed into cuvettes using sterile tweezers and subjected to electroporation according to the parameters outlined in Table 1. Gels were subsequently transferred back into wells containing fresh culture medium and incubated at 37°C with 5% carbon dioxide.

To account for possible artifacts due to sample manipulation or device handling, a sham pulse condition was also included as a control. A PI-treated 3D-printed construct was placed inside the cuvette following the same procedure as the experimental samples, and the electroporation device was operated with the voltage set to 0 V (no electroporation), ensuring that no electrical pulse was delivered. This control allowed verification that PI uptake observed in the electroporation group was attributable solely to electroporation.

After 1 hour, to allow cells to return to baseline conditions,[40,41] DAPI staining was performed to visualize nuclei and confirm PI diffusion within the gel and uptake by electroporated cells. The PI uptake assay was performed in duplicate.

2.8. Programmed death-ligand 1 immunoassay in 2D and 3D bioprinted FaDu cultures

Programmed death-ligand 1 is an immune checkpoint protein frequently expressed in various tumor types, including HNSCCs, where it plays a crucial role in immune evasion. PD-L1 expression has been confirmed in FaDu cells cultured under standard 2D conditions.[33] It is also essential to verify, in the 3D bioprinted system, that the bioprinting process does not alter key phenotypic markers such as PD-L1. Therefore, the immunoassay was performed in both 2D and 3D FaDu cultures to validate the preservation of PD-L1, ensuring the biological relevance of the model for studies of immune interactions and programmed death-1/PD-L1-targeted therapies.

For PD-L1 assessment, a total of six structures were bioprinted (three without electroporation and three with electroporation). At 14 and 21 days (n = 3 per time point), structures were washed with MilliQ water and fixed with 4% paraformaldehyde (200 μL) for 10 minutes at room temperature, followed by two washes with MilliQ water (one minute each). Permeabilization was performed using 0.1% Triton™ X-100 (200 μL) for 15 minutes, followed by two additional washes. Blocking was performed using 2%

bovine serum albumin (BSA, 200 µL) for one hour at room temperature to prevent nonspecific binding.

After blocking, cells were incubated overnight at 4°C with PD-L1 polyclonal primary antibody (#PA5-20343, Thermo Fisher Scientific, United States) diluted 1:100 in 0.1% BSA (200 µL). The following day, cells were washed twice with MilliQ water and incubated for 45 minutes at room temperature with Alexa Fluor 647 goat anti-rabbit secondary antibody (A21245, Thermo Fisher Scientific, United States), diluted 1:2000 in 0.1% BSA.

Nuclei were counterstained using ProLong™ Diamond Antifade Mountant (Thermo Fisher Scientific, United States) with DAPI, and the F-actin cytoskeleton was stained with Alexa Fluor™ 488 Phalloidin (A12379, Thermo Fisher Scientific, United States) at a 1:300 dilution. All images were acquired using an immunofluorescence microscope. FaDu cells cultured in 2D were used as controls. The assay was performed in duplicate.

Fluorescence quantification of PD-L1 signal intensity was performed using a custom MATLAB script (R2023a, The MathWorks Inc., United States) to ensure unbiased and reproducible analysis across 2D and 3D samples. The script extracted the mean grayscale intensity from each immunofluorescence image after optional cropping to remove noninformative regions (e.g., borders & scale bars). For each experimental group, the code computed the average fluorescence intensity and standard deviation across replicates. Images were first converted to grayscale when needed, and intensity values were derived from the mean pixel intensity over the entire field of view. Groups and file paths were predefined in the MATLAB structure, allowing automated batch processing and preventing operator bias. Example MATLAB code used for intensity extraction is provided in the **Supplementary File**.

2.9 Statistical analysis

Statistical comparisons among groups were conducted using an ordinary one-way analysis of variance with a single pooled variance, followed by Tukey's multiple comparisons test. Data normality was assessed using the Shapiro–Wilk test. To ensure reproducibility, each experiment was independently repeated at least three times. A p-value ≤ 0.05 was considered statistically significant. Significance thresholds were indicated as follows: $p < 0.05$ (*) and $p < 0.001$ (**). GraphPad prims v. 10.6.1

3. Results

3.1 Osmotic and mechanical characterization of biomaterial ink

The osmolarity of the $CaCl_2$ crosslinking solutions was calculated using **Equation (1)** to assess compatibility with physiological conditions, particularly for subsequent cell encapsulation. The calculated values for 0.5%, 1%, and 2% wt $CaCl_2$ were 0.135, 0.270, and 0.541 Osm/L, respectively, showing a progressive increase with salt concentration. The 1% wt solution was closest to physiological osmolarity (~0.290 Osm/L), while the 0.5% wt solution was hypotonic

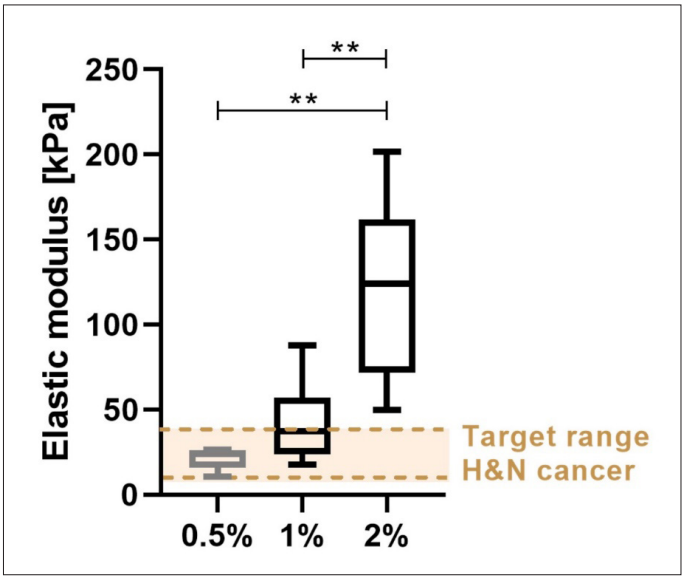

Figure 3. Mechanical characterization of sodium-alginate–gelatin hydrogels crosslinked with different calcium chloride ($CaCl_2$) concentrations. Box plots show the elastic modulus of hydrogels crosslinked with 0.5%, 1%, and 2% $CaCl_2$. Increasing the CaCl2 concentration resulted in a significant increase in stiffness ($n = 3$ independent batches, each containing 10 specimens, for a total of $n = 30$, $^{**}p < 0.001$). The shaded region represents the reported elastic modulus range of non-mineralized head and neck tumor (H&N) tissue, used as a target mechanical range for model optimization.

and the 2% wt solution hypertonic, indicating potential impacts on cell homeostasis during crosslinking.

The stiffness of the SA–GEL samples crosslinked with 0.5%, 1%, and 2% wt $CaCl_2$ was evaluated to replicate the mechanical environment of head and neck tumor tissue, which has an elastic modulus reported between 10 and 38 kPa.[13,42] Mechanical testing revealed clear differences between $CaCl_2$ concentrations (Figure 3). Samples crosslinked with 0.5% wt $CaCl_2$ exhibited the lowest modulus (21.65 ± 6.56 kPa), 1% wt samples showed 42.96 ± 19.89 kPa, and 2% wt samples reached 117.11 ± 45.83 kPa. Statistical analysis indicated a significant difference between 1% and 2% wt ($p < 0.0001$), while the 0.5% and 1% wt groups were not significantly different.

Both the 0.5% and 1% wt samples were within or near the reported physiological range for head and neck tumors, whereas the 2% wt samples substantially exceeded it. These results confirm that increasing $CaCl_2$ concentration correlates with increased stiffness, consistent with previous reports on alginate-based hydrogels.[43]

From a practical perspective, 0.5% wt samples were mechanically fragile and prone to handling difficulties during subsequent electroporation experiments. Considering stiffness, osmolarity, and structural integrity, the 1% wt $CaCl_2$ was selected for all further experiments.

3.2. 3D bioprinted head and neck squamous cell carcinoma model for electroporation

The 3D bioprinted tumor models consisted of rectangular, multilayer hydrogel structures produced using the SA–GEL bioink. Each structure measured 10 × 30 mm with a thickness of 1.05 mm, resulting in a mechanically stable structure suitable for electroporation testing. This geometry ensured uniform layer deposition and provided a reproducible platform for subsequent biological and electroporation analyses.

To evaluate electroporation compatibility, two thicknesses were printed: 1.05 mm (3L-SA–GEL) and 1.3 mm (4L-SA–GEL), both designed to fit inside the cuvette. Electroporation was performed at 200 V and 300 V. Results (Figure 4A) show that the thinner 3L-SA–GEL structure allowed efficient current conduction at both voltages, while the thicker 4L-SA–GEL structure impeded current conduction at 300 V and allowed only partial conduction at 200 V, with reduced current relative to the applied voltage. These results indicate that the 3L-SA–GEL configuration is optimal for electroporation experiments.

3.3. Morphological characterization of 3D bioprinted structures

To assess the uniformity of the 3D-printed structures, they were lyophilized and weighed using an analytical balance. The consistent weight of the dried structures (45.2 ± 1.77 mg) confirmed the reproducibility of the printing process and uniform extrusion of the bioink. Morphological characterization using SEM revealed a dense and compact surface structure (Figure 4B & C), while cross-sectional images showed interconnected pores that support cell proliferation and interaction (Figure 4D & E). Porosity and average pore area were quantified using a custom MATLAB script (R2023a, The MathWorks Inc., United States). The structures exhibited 43.8 ± 5.9% porosity, with an average pore area of 109.21 ± 33.3 μm^2.

3.4. FaDu cell incorporation in 3D bioprinted structures

To evaluate the impact of electroporation on cell viability, FaDu cells were incorporated into SA–GEL, bioprinted, and subsequently subjected to electroporation. Cell viability and proliferation were monitored for up to 21 days in culture. Viability remained consistently 80% (± 5%) across all time points, indicating a largely healthy cell population under the experimental conditions. By day 21, an increase in cell death was observed, as evidenced by red-stained nuclei, likely reflecting normal turnover or stress at later stages of development.

Despite this, the cells organized into aggregates, forming structures similar to spheroids (Figure 5E & F), a hallmark of tumor cell behavior.[44] DAPI staining further confirmed that cells within the structures formed clusters/spheroids ranging from 85.89 µm to 459.37 µm, with a mean diameter of 302.71 ± 112.62 µm (Figure 6). These structures are characteristic of tumor cell clusters, supporting the ability of FaDu cells to self-organize into 3D spheroids, effectively recapitulating tumor-like behavior.[45]

Electroporation did not compromise cell viability, suggesting that the procedure did not induce significant stress or damage.

3.5. Propidium iodide uptake in 3D bioprinted structure under electroporation

To evaluate the suitability of the 3D bioprinted model for testing electroporation efficiency, the hydrophilic model molecule PI was used. PI cannot cross intact cell membranes, making it a reliable indicator of transient pore formation during electroporation. This experiment aimed to confirm that the hydrogel permits the diffusion of molecules through the printed structure and that electroporation effectively permeabilizes the cell membranes.

Figure 7 shows the results at 14 and 21 days of incubation of FaDu-loaded 3D hydrogel structures treated with PI. Samples exposed to PI without electroporation exhibited no red fluorescence, indicating that PI was not internalized (Figure 7A, 7B and 7E, 7F). In contrast, electroporated

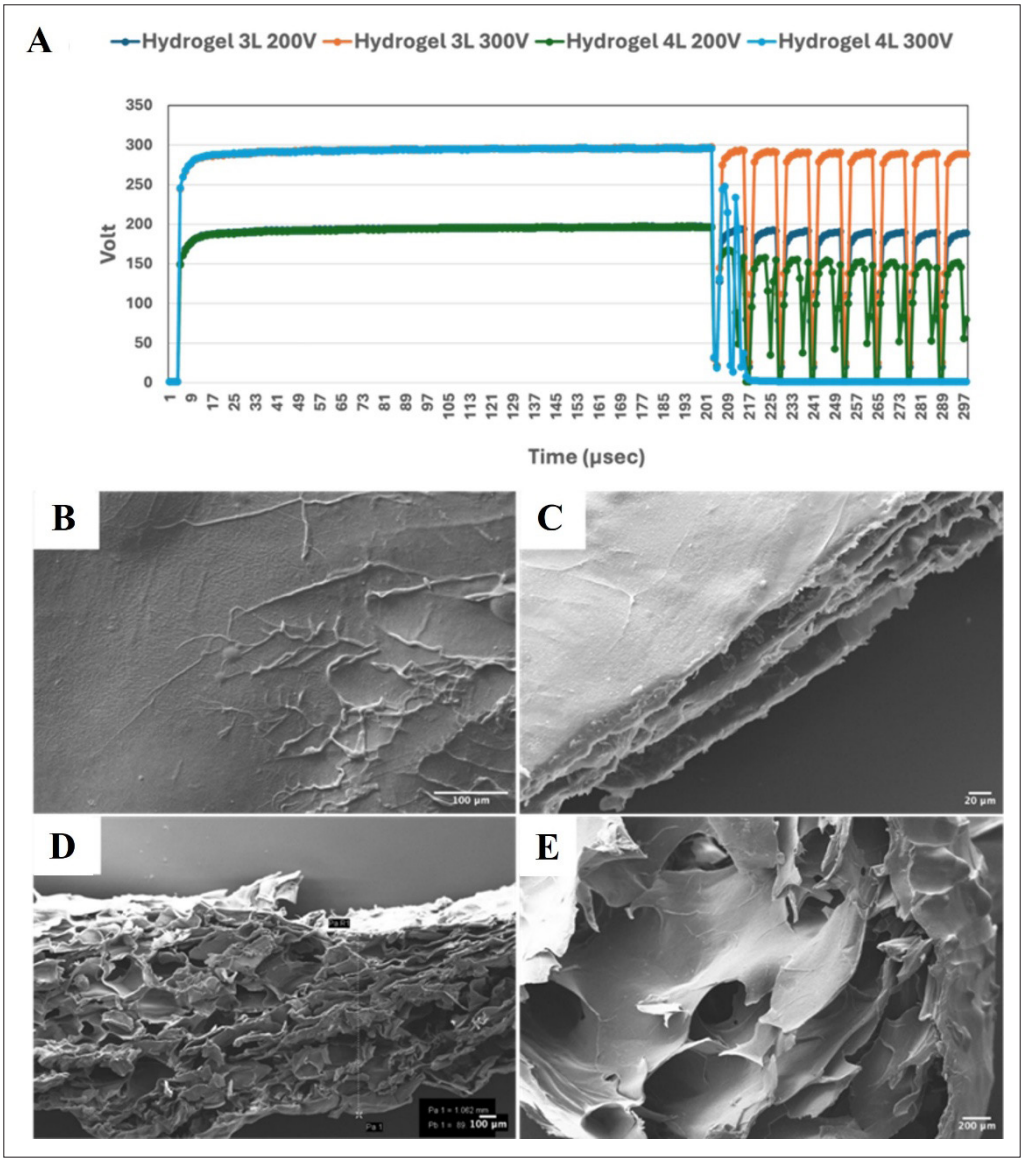

Figure 4. Electroporation pulse profiles and microstructural characterization of sodium alginate (SA)–gelatin (GEL) hydrogels. (A) Results of the electroporation test on the three-layer (3L)-SA–GEL (red & blue lines) and the four-layer (4L)-SA–GEL (green & orange lines) at 200 V and 300 V. Before applying electroporation pulses to cells, a constant voltage was applied to verify current conduction through the hydrogel; no cells were present during this pre-test. (B) Scanning electron microscopy image of 3L-SA–GEL surface morphology. Scale bar: 100 μm; magnification: 1000×. (C) Scanning electron microscopy cross-section showing internal porosity. Scale bar: 20 μm; magnification: 120,000×. (D) Frontal cross-section with visible layered structure. Scale bar: 100 μm; magnification: 120,000×. (E) Inner cross-sections highlighting layer interconnections of the three-dimensional bioprinted structure. Scale bar: 200 μm; magnification: 1000×.

samples exhibited clear red fluorescence (Figure 7C, 7D & 7G, 7H), with DAPI nuclear staining confirming that the red signal originated from PI internalization into the cells.

These results demonstrate that the 3D bioprinted head and neck tumor model can effectively serve as a platform for evaluating electroporation-mediated molecule uptake, supporting its potential use in screening electroporation-drug conjugates.

3.6. Programmed death-ligand 1 immunoassay in 2D and 3D bioprinted FaDu cultures

Fluorescence microscopy images were used to assess PD-L1 expression in FaDu cells under different culture conditions and time points. Figures 8A–D and 8E–H show representative images acquired at 14 and 21 days, respectively. FaDu control cells grown in 2D culture (Figure 8A, B, E, F) displayed baseline PD-L1 expression, with PD-

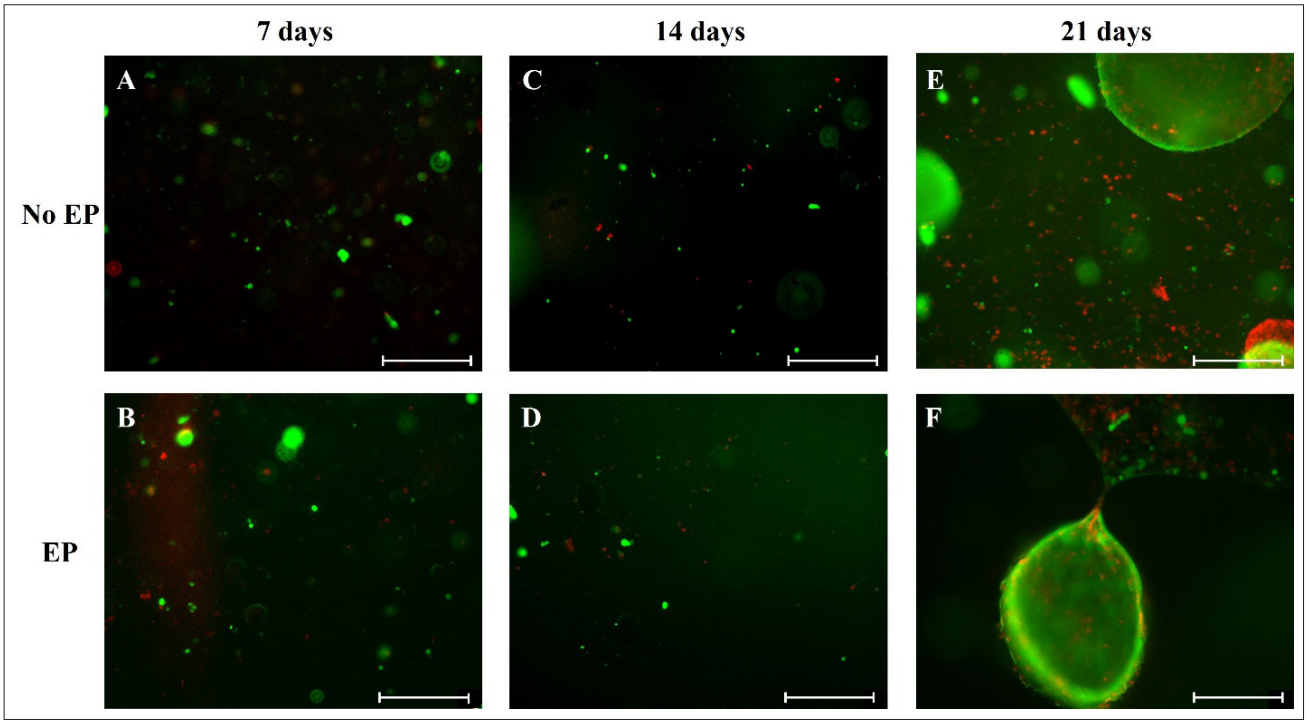

Figure 5. Long-term viability of three-dimensional (3D) bioprinted tumor constructs following electroporation (EP). Live/Dead fluorescence images of 3D SA–GEL bioprinted hydrogels, either untreated (no EP) or subjected to EP, and evaluated at three time points: (A, B) 7 days, (C, D) 14 days, and (E, F) 21 days. Green fluorescence indicates live cells, while red fluorescence marks dead cells. Across all time points, constructs maintained overall viability and supported progressive cluster formation. Scale bar: 100 μm; magnification: 10,000×.

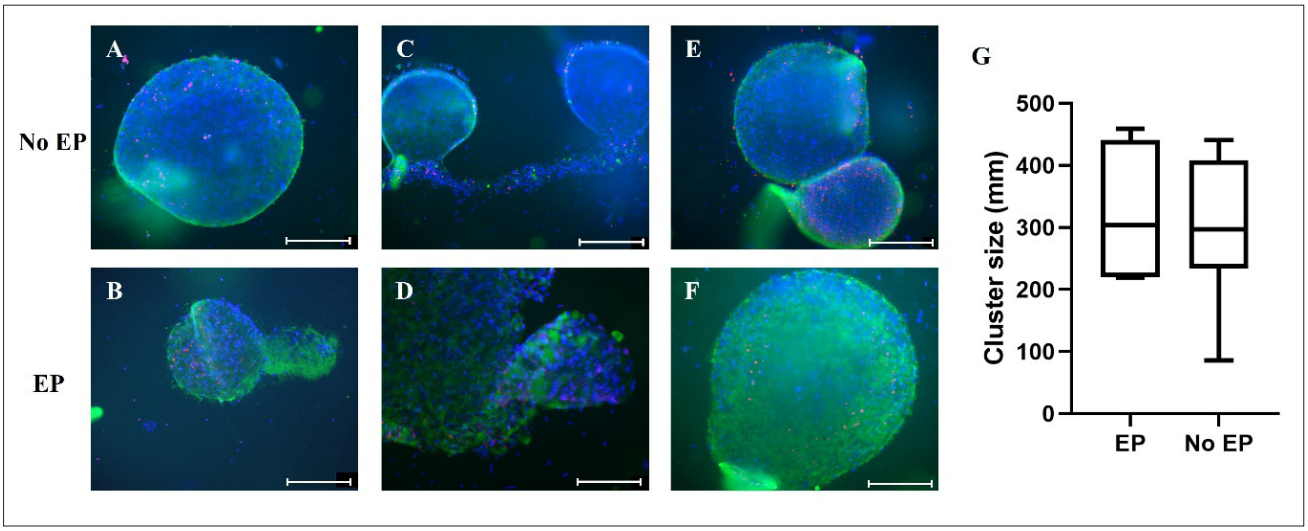

Figure 6. Cluster formation within the three-dimensional (3D) bioprinted head and neck tumor model. Live/Dead and 4',6-diamidino-2-phenylindole staining of 3D bioprinted constructs cultured for 21 days, shown for conditions without electroporation (no electroporation [EP]; A, C, E) and with EP (B, D, F). Panels A–F represent clusters imaged from different samples collected at the same 21-day time point. (G) Cluster diameters range from 85.89 to 459.37 μm. Green: live cells; red: dead cells; blue: cell nuclei. Scale bar: 100 μm; magnification: 10×.

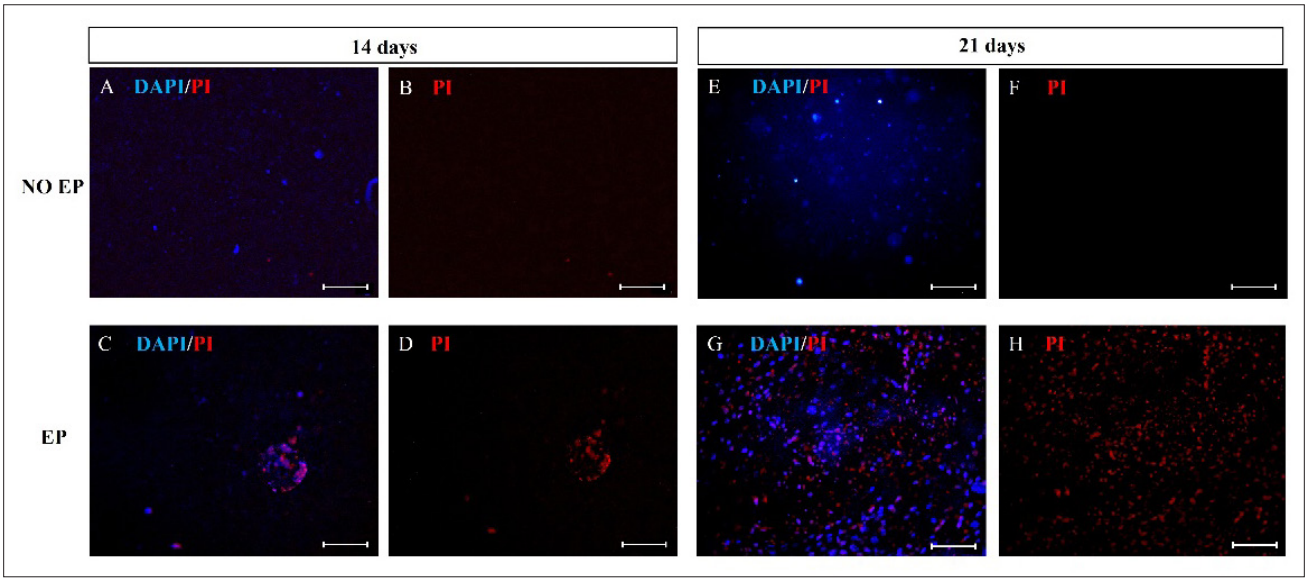

Figure 7. Electroporation enhances propidium iodide (PI) uptake in three-dimensional (3D) bioprinted structures. Fluorescence images of 3D bioprinted hydrogels with FaDu cells after 14 and 21 days of incubation following PI treatment. Non-electroporated samples (no EP; A, B, E, F) show no detectable PI signal, indicating the absence of dye internalization. In contrast, electroporated (EP; C, D, G, H) samples exhibit clear red fluorescence, confirming effective membrane permeabilization and the uptake of PI. 4',6-diamidino-2-phenylindole (DAPI) nuclear staining verifies the intracellular localization of PI. These findings demonstrate that the 3D bioprinted head and neck tumor model is suitable for evaluating electroporation-mediated molecular delivery.

L1 staining visualized in red. FaDu cells embedded in the 3D hydrogel showed time-dependent changes in PD-L1 expression (Figure 8 C,D,G & H). When cluster formation occurred within the 3D model, PD-L1 expression was higher compared to the same time points in 2D culture.

This upregulation likely reflects the more physiologically relevant tumor-like microenvironment of the 3D system, where enhanced cell–cell and cell–matrix interactions, as well as localized hypoxic and mechanical cues, activate immune evasion pathways absent in conventional 2D monolayers. PD-L1 localization appears as red fluorescence, with intensity differences observable between experimental groups and time points. Figure 8I quantitatively summarizes the mean PD-L1 fluorescence intensity for each condition, measured through image analysis of stained samples. The results indicate an overall increase in PD-L1 expression at 21 days in the 3D-printed gel compared to 2D controls, with error bars reflecting variability among replicates.

4. Discussion

The present study introduces a novel, physiologically relevant 3D bioprinted *in vitro* model of head and neck cancer, specifically engineered for electroporation research. This platform addresses the critical need for preclinical systems that replicate both the mechanical and biological tumor microenvironment while enabling high-throughput evaluation of electric field-based therapies and intracellular drug delivery. Unlike previous models, our system uniquely combines mechanical tunability, compatibility with electroporation, and immune biomarker expression within a single, reproducible platform.[14,15]

A central feature of the model is the tunable mechanical properties achieved through controlled $CaCl_2$ crosslinking. Mechanical characterization revealed a clear dependence of elastic modulus on $CaCl_2$ concentration. Samples crosslinked with 0.5% wt $CaCl_2$ exhibited the lowest stiffness (21.65 ± 6.56 kPa), while 1% wt samples reached 42.96 ± 19.89 kPa, and 2% wt samples were significantly stiffer (117.11 ± 45.83 kPa). Statistical analysis confirmed that the difference between 1% and 2% wt $CaCl_2$ is significant ($p < 0.0001$), whereas the difference between 0.5% and 1% wt was not statistically significant, indicating that the moderate increase in crosslinker concentration from 0.5% to 1% wt does not produce a proportional change in stiffness within experimental variability. Both the 0.5% wt and 1% wt samples were within or close to the reported physiological range of head and neck tumors (10–38 kPa).[13,42] Specifically, the 0.5% wt samples fell near the midpoint of this range and may provide the most accurate mechanical match to the native tumor stiffness. However, as noted in our results, the 0.5% wt hydrogels were mechanically fragile, difficult to handle, and hypotonic (~0.135 Osm/L), which could compromise cell

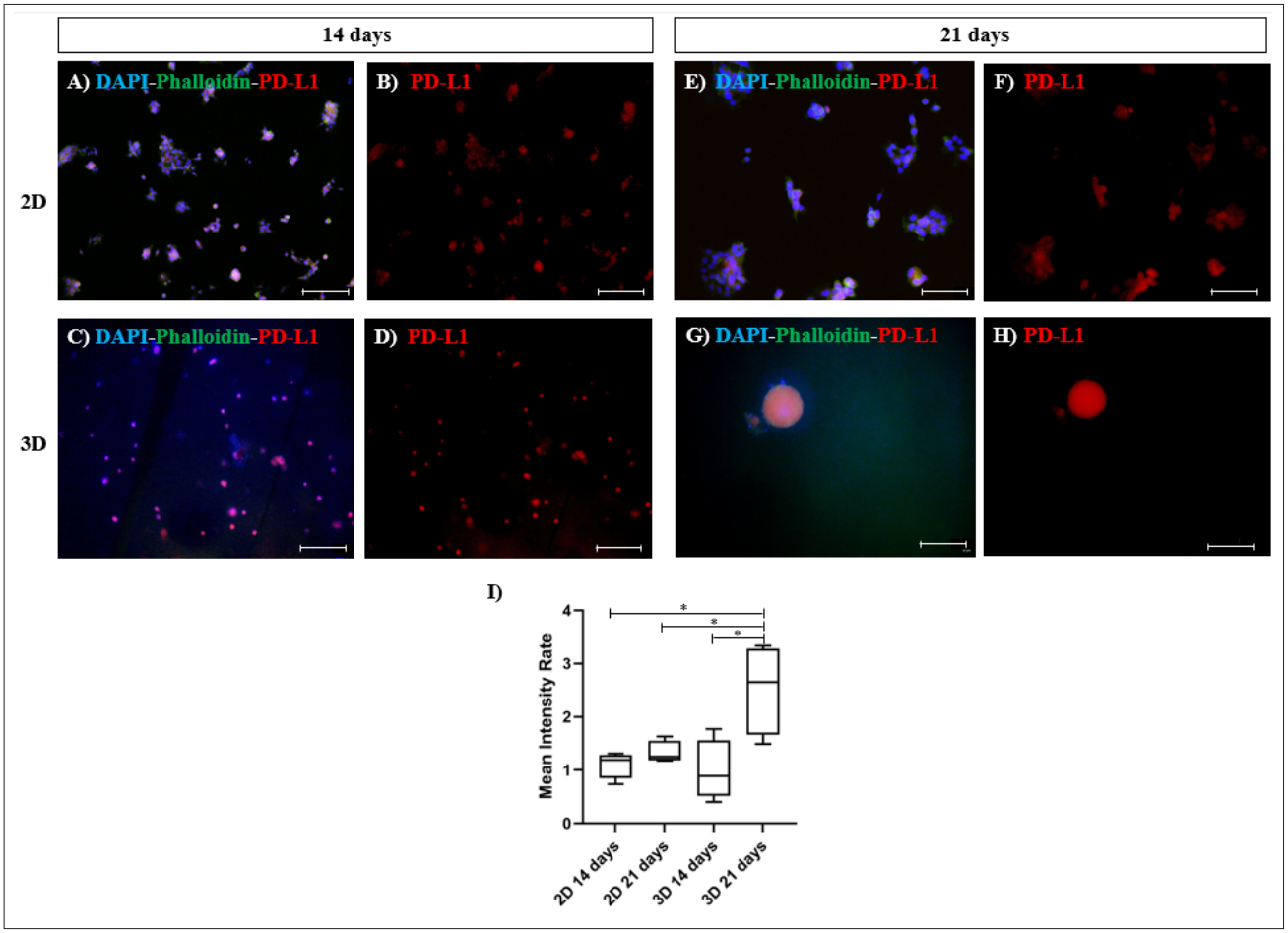

Figure 8. Time-dependent modulation of programmed death-ligand 1 (PD-L1) expression in two-dimensional (2D) versus three-dimensional (3D) bioprinted FaDu cultures. Representative fluorescence images of PD-L1 immunostaining in FaDu cells cultured in a 2D monolayer (A, B, E, F) and laden in a 3D bioprinted structure (C, D, G, H) after 14 and 21 days. PD-L1 expression (red) remains low in 2D cultures at both time points, whereas 3D bioprinted constructs show a progressive increase in PD-L1 signal—most notably at day 21, coinciding with the development of multicellular tumor-like clusters. Quantitative analysis (I) confirms significantly higher PD-L1 fluorescence intensity in 3D samples at 21 days compared to 2D controls (*$p < 0.05$), indicating activation of immune-evasion-related pathways within the 3D tumor microenvironment. Nuclei are counterstained with 4',6-diamidino-2-phenylindole (DAPI; blue). Scale bar: 100 μm; magnification: 10×.

viability, particularly during electroporation procedures.[46] In contrast, the 2% wt samples were hypertonic (~0.541 Osm/L) and substantially stiffer than typical head and neck tumor tissue, which could alter cell behavior and mechanotransduction pathways. The 1% wt $CaCl_2$ formulation emerged as an optimal compromise, providing an elastic modulus of 43 kPa, moderate osmolarity (~0.27 Osm/L), and sufficient mechanical integrity for reliable handling and electroporation experiments. These findings align with previous reports showing that increased $CaCl_2$ crosslinking enhances alginate hydrogel stiffness[43] and are consistent with the well-documented heterogeneity of head and neck tumor mechanics, which can vary due to anatomical origin, ECM composition, and remodeling.[47-49] For example, head and neck cancers can arise in multiple sites (oral cavities, larynx, pharynx) and encompass a wide range of primary and metastatic cell lines, contributing to the observed variability in elastic modulus.[48] Additionally, abnormal ECM deposition and altered mechanotransduction pathways in tumors can further expand the spectrum of stiffness.[49] While the 1% wt $CaCl_2$ hydrogel balances mechanical properties, osmolarity, and handling considerations, it does not fully capture the mechanical heterogeneity present in native tumors. The 0.5% wt formulation, although closer to the center of the physiological range, may be too fragile and hypotonic for practical use. Conversely, 2% wt samples, although robust, exceeded physiological stiffness and osmolarity, which could influence cell responses. Future studies should incorporate stiffness gradients and co-culture systems to more accurately recapitulate the tumor microenvironment.

Electroporation experiments confirmed that the 3D structures can sustain current conduction under applied electric fields without structural compromise, particularly in the 3L-SA–GEL configuration, demonstrating the feasibility of electroporation in a 3D bioprinted head and neck system. This finding is crucial because 3D matrices often lose conductivity due to thickness or dehydration-induced resistance. The electrical characterization of the hydrogel should be addressed in future work through a dedicated study specifically designed to evaluate its electrical properties and response under various electroporation conditions, including field distribution, pore formation, and molecular transport, thereby enhancing the predictive capability for ECT applications.

Morphological and porosity analyses confirmed a porous, interconnected microarchitecture (~44% porosity, ~109 μm^2 average pore area), which supports nutrient diffusion, waste removal, and cellular infiltration. These features closely mimic the tumor ECM, facilitating 3D cell organization, mechanotransduction, and more physiologically relevant drug and immune signaling responses. It should be noted, however, that the freeze-drying process employed in this study may have caused partial collapse of the hydrogel microstructure. Future work should implement critical point drying or cryo-SEM to more accurately preserve the native architecture and better evaluate the true pore structure of the constructs.

Preliminary biological validation demonstrated sustained FaDu cell viability for up to 21 days, with spheroid formation closely resembling native tumor clusters (85–459 μm). Electroporation did not significantly reduce viability (approximately 75–80% live cells), demonstrating the robustness of the model. The observed trends should be interpreted as preliminary evidence of biocompatibility rather than conclusive biological outcomes, and further validation using quantitative viability assays, live/dead 3D imaging, and molecular markers of membrane repair is still required. These findings confirm that electroporation can be safely applied in this model, facilitating cell permeabilization and potentially enabling drug delivery applications.

Functional validation of electroporation was confirmed by the intracellular uptake of PI, which occurred only after application of electric pulses. The detection of PI fluorescence inside the cells indicates that the dye—normally impermeable to intact membranes—penetrated the cells, confirming the transient formation of membrane pores. Although the pores themselves are not directly visualized, their transient formation can be inferred from PI internalization. These findings demonstrate that the hydrogel does not hinder electric field propagation, supporting the utility of this model for testing the intracellular delivery of hydrophilic molecules, including therapeutic agents and gene-editing tools. Moreover, the selected electroporation parameters ensured reversible membrane permeabilization without cytotoxicity.[8]

Another key validation is the model's ability to recapitulate the dynamics of tumor-associated biomarkers. PD-L1 expression increased over time in the 3D-printed structures compared to 2D controls (~1.5–2-fold, Figure 8I). This observation aligns with previous studies, where PD-L1 upregulation is linked to enhanced cell–cell and cell–ECM interactions, hypoxia, and other tumor microenvironment stressors.[33] This underscores the importance of spatial and mechanical cues in regulating immune checkpoint pathways, highlighting the model's potential as a platform for screening immunomodulatory treatments, including checkpoint inhibitors.

Comparison with existing 3D HNSCC models, such as Azhakesan *et al.*,[19] highlights the novelty of our system. While prior models demonstrated long-term viability and responsiveness to radiochemotherapy, our platform uniquely integrates mechanical properties, electroporation compatibility, and immune biomarker expression, enabling functional validation of electric field-mediated intracellular delivery. Unlike Azhakesan *et al.*,[19] we quantitatively benchmarked hydrogel stiffness (10–38 kPa) against native tumor tissue, which is critical for electroporation efficiency as both electric field propagation and membrane response are influenced by matrix mechanics.[50]

In summary, this 3D bioprinted head and neck model combines reproducible mechanical properties, structural integrity, electroporation functionality, and physiologically relevant tumor behaviors. While full quantitative mapping of electric fields and extended biological assays remain areas for future work, the platform represents a scalable, modular, and physiologically relevant system suitable for preclinical investigation of ECT and immunomodulatory strategies.

5. Conclusion

To our knowledge, this study presents the first 3D bioprinted *in vitro* model of head and neck cancer specifically designed for electroporation research, providing a physiologically relevant platform for preclinical testing. By optimizing the $CaCl_2$ concentration to 1% wt, the hydrogel achieved a stiffness closely matching that of native head and neck tissue, ensuring a mechanically relevant microenvironment. The bioprinted structures demonstrated high reproducibility, structural integrity, and robust handling, supporting complex procedures like electroporation.

The model also supports key tumor-like behaviors, including sustained cell viability, 3D spheroid formation, and PD-L1 expression. Electroporation experiments confirmed effective current conduction under applied electric fields without compromising cell health, validating the system for intracellular delivery studies.

By bridging the gap between 2D cultures and *in vivo* models, this 3D bioprinted platform offers a scalable, tunable, and physiologically relevant system for investigating tumor biology, testing therapies, and advancing personalized treatment strategies. Future work should include quantitative mapping of electric fields and expanded biological validation, further enhancing its predictive value and utility in preclinical research.

Acknowledgments

The authors would like to express their gratitude to IGEA Medical, Italy, for the Genedrive electroporator apparatus.

Funding

The work reported in this publication was funded by the Italian Ministry of Health, RC-2021 grant #08053922 under the project, "Nano-Electro-Chemo-Immuno Therapy (NECIT) to enhance head and neck cancer treatment." This study was also supported by the Italian Ministry of Education, University and Research and the University of Pavia within the Departments of Excellence 2023–2027 program , as well as by the Ministry of Enterprise and Made in Italy.

Conflict of interest

The authors declare they have no competing interests.

Author contributions

Conceptualization: Franca Scocozza, Silvia Pisani
Formal analysis: Franca Scocozza, Silvia Pisani, Aleksandra Evangelista
Investigation: Franca Scocozza, Silvia Pisani, Aleksandra Evangelista
Methodology: Franca Scocozza, Silvia Pisani, Aleksandra Evangelista
Writing – original draft: Franca Scocozza, Silvia Pisani, Aleksandra Evangelista
Writing – review & editing: Ferdinando Auricchio, Michele Conti, Bice Conti, Marco Benazzo

Ethics approval and consent to participate

Not applicable.

Consent for publication

Not applicable.

Availability of data

All data analyzed have been presented in the paper. The raw datasets (e.g., mechanical testing curves) can be provided upon request.

Further disclosure

Preliminary results from this study were presented at the 1° Workshop: "From 3D Printing to 3D Bioprinting – an opportunity for preclinical and clinical applications at GSD held in IRCCS S. Raffaele, Milan on 27/10/2025

References

1. Chow Laura QM. Head and Neck Cancer. *J Clin Med*. 2020;382(1):60-72.
doi: 10.1056/NEJMra1715715

2. Pisani P, Airoldi M, Allais A, *et al*. Metastatic disease in head & neck oncology. *Acta Otorhinolaryngol Ital*. 2020;40(Suppl. 1):S1-s86.
doi: 10.14639/0392-100X-suppl.1-40-2020

3. Anderson G, Ebadi M, Vo K, Novak J, Govindarajan A, Amini A. An Updated Review on Head and Neck Cancer Treatment with Radiation Therapy. *Cancers (Basel)*. 2021;13(19):4912.
doi: 10.3390/cancers13194912

4. Debela DT, Muzazu SG, Heraro KD, *et al*. New approaches and procedures for cancer treatment: Current perspectives. *SAGE Open Med*. 2021;9:20503121211034366.
doi: 10.1177/20503121211034366

5. Wang H, Zheng Z, Zhang Y, *et al*. Locally advanced head and neck squamous cell carcinoma treatment efficacy and safety: a systematic review and network meta-analysis. Review. *Front Pharmacol*. 2023;14:1269863.
doi: 10.3389/fphar.2023.1269863

6. Condello M, D'Avack G, Spugnini EP, Meschini S. Electrochemotherapy: An Alternative Strategy for Improving Therapy in Drug-Resistant SOLID Tumors. *Cancers (Basel)*. 2022;14(17):4341.
doi: 10.3390/cancers14174341

7. Zupanic A, Kos B, Miklavcic D. Treatment planning of electroporation-based medical interventions: electrochemotherapy, gene electrotransfer and irreversible electroporation. *Physics in Medicine & Biology*. 2012; 57(17):5425.
doi: 10.1088/0031-9155/57/17/5425

8. Gehl J, Sersa G, Matthiessen LW, *et al*. Updated standard operating procedures for electrochemotherapy of

cutaneous tumours and skin metastases. *Acta Oncol*. 2018;57(7):874-882.
doi: 10.1080/0284186x.2018.1454602

9. Gehl J, Sersa G, Garbay J, *et al*. Results of the ESOPE (European Standard Operating Procedures on Electrochemotherapy) study: Efficient, highly tolerable and simple palliative treatment of cutaneous and subcutaneous metastases from cancers of any histology. *J Clin Oncol*. 2006;24(18_suppl):8047-8047.
doi: 10.1200/jco.2006.24.18_suppl.8047

10. Martya M, Sersab G, Garbaya J-R, *et al*. Electrochemotherapy – An easy, highly effective and safe treatment of cutaneous and subcutaneous metastases: Results of ESOPE (European Standard Operating Procedures of Electrochemotherapy) study. *Ejc Supplements*. 2006;4:3-13.

11. Calvet CY, Mir LM. The promising alliance of anti-cancer electrochemotherapy with immunotherapy. *Cancer Metastasis Rev*. 2016;35(2):165-77.
doi: 10.1007/s10555-016-9615-3

12. Abuwatfa WH, Pitt WG, Husseini GA. Scaffold-based 3D cell culture models in cancer research. *J Biomed Sci*. 2024;31(1):7.
doi: 10.1186/s12929-024-00994-y

13. Evangelista A, Scocozza F, Conti M, *et al*. Exploring Mechanical Features of 3D Head and Neck Cancer Models. *J Funct Biomater*. 2025;

14. Ding Y, Chen J, Zhong W, Gu T, Xiao Y, Zhao Z. Bioprinting in tumor model construction for head and neck squamous cell carcinoma: A review. *IJB*. 2025;11(2):139–163.
doi: 10.36922/ijb.8100

15. Meng F, Meyer CM, Joung D, Vallera DA, McAlpine MC, Panoskaltsis-Mortari A. 3D Bioprinted *In vitro* Metastatic Models via Reconstruction of Tumor Microenvironments. *Adv Mater*. 2019;31(10):1806899.
doi: 10.1002/adma.201806899

16. Ng WL, Vyas C, Huang B, Yeong WY, Bartolo P. Advanced bioprinting strategies for fabrication of biomimetic tissues and organs. *IJEM*. 2025;7(6):062006.
doi: 10.1088/2631-7990/adeee0

17. Cui X, Jiao J, Yang L, *et al*. Advanced tumor organoid bioprinting strategy for oncology research. *Mater Today Bio*. 2024;28:101198.
doi: 10.1016/j.mtbio.2024.101198

18. Kort-Mascort J, Bao G, Elkashty O, *et al*. Decellularized Extracellular Matrix Composite Hydrogel Bioinks for the Development of 3D Bioprinted Head and Neck *in vitro* Tumor Models. *ACS Biomater Sci Eng*. 2021;7(11): 5288-5300.
doi: 10.1021/acsbiomaterials.1c00812

19. Azhakesan A, Kern J, Mishra A, *et al*. 3D Bioprinted Head and Neck Squamous Cell Carcinoma (HNSCC) Model Using Tunicate Derived Nanocellulose (NC) Bioink. *Adv Healthc Mater*. 2025:14:e2403114.
doi: 10.1002/adhm.202403114

20. Kort-Mascort J, Shen ML, Martin E, *et al*. Bioprinted cancer-stromalin-vitromodels in a decellularized ECM-based bioink exhibit progressive remodeling and maturation. *Biomed Mater*. 2023;18(4):045022.
doi: 10.1088/1748-605X/acd830

21. Delgrosso E, Scocozza F, Cansolino L, *et al*. 3D bioprinted osteosarcoma model for experimental boron neutron capture therapy (BNCT) applications: Preliminary assessment. *J Biomed Mater Res Part B: Applied Biomater*. 2023;111(8):1571-1580.
doi: 10.1002/jbm.b.35255

22. Wang X, Yang Y, Hu X, Kawazoe N, Yang Y, Chen G. Morphological and Mechanical Properties of Osteosarcoma Microenvironment Cells Explored by Atomic Force Microscopy. *Anal Sci*. 2016;32(11):1177-1182.
doi: 10.2116/analsci.32.1177

23. Xu W, Mezencev R, Kim B, Wang L, McDonald J, Sulchek T. Cell stiffness is a biomarker of the metastatic potential of ovarian cancer cells. *PLoS One*. 2012;7(10):e46609.
doi: 10.1371/journal.pone.0046609

24. Esch M, Sukhorukov VL, Kürschner M, Zimmermann U. Dielectric properties of alginate beads and bound water relaxation studied by electrorotation. *Biopolymers*. 1999;50(3):227-37.
doi: 10.1002/(sici)1097-0282(199909)50:3<227::Aid-bip1>3.0.Co;2-y

25. Kaklamani G, Kazaryan D, Bowen J, Iacovella F, Anastasiadis SH, Deligeorgis G. On the electrical conductivity of alginate hydrogels. *Regen Biomater*. 2018;5(5):293-301.
doi: 10.1093/rb/rby019

26. Distler T, Polley C, Shi F, *et al*. Electrically Conductive and 3D-Printable Oxidized Alginate-Gelatin Polypyrrole:PSS Hydrogels for Tissue Engineering. *Adv Healthc Mater*. 2021;10(9):e2001876.
doi: 10.1002/adhm.202001876

27. Tordi P, Tamayo A, Jeong Y, Bonini M, Samorì P. Multiresponsive Ionic Conductive Alginate/Gelatin Organohydrogels with Tunable Functions. *Adv Funct Mater*. 2024;34(52):2410663.
doi: 10.1002/adfm.202410663

28. Ji D, Park JM, Oh MS, *et al*. Superstrong, superstiff, and conductive alginate hydrogels. *Nat Commun*. 2022;13(1):3019.
doi: 10.1038/s41467-022-30691-z

29. Massey A, Stewart J, Smith C, *et al*. Mechanical properties of human tumour tissues and their implications for cancer development. *Nat Rev Phys*. 2024;6(4): 269-282.
doi: 10.1038/s42254-024-00707-2

30. Bergman E, Goldbart R, Traitel T, *et al*. Cell stiffness predicts cancer cell sensitivity to ultrasound as a selective superficial cancer therapy. *Bioeng Transl Med*. 2021;6(3):e10226. doi: 10.1002/btm2.10226

31. Almela T, Tayebi L, Moharamzadeh K. 3D bioprinting for *in vitro* models of oral cancer: Toward development and validation. *Bioprint*. 2021;22:e00132. doi: 10.1016/j.bprint.2021.e00132

32. Ragazzini S, Scocozza F, Bernava G, *et al*. Mechanosensor YAP cooperates with TGF-β1 signaling to promote myofibroblast activation and matrix stiffening in a 3D model of human cardiac fibrosis. *Acta Biomater*. 2022;152: 300-312. doi: 10.1016/j.actbio.2022.08.063

33. Kulasinghe A, Kenny L, Punyadeera C. Circulating tumour cell PD-L1 test for head and neck cancers. *Oral Oncol*. 2017;75:6-7. doi: 10.1016/j.oraloncology.2017.10.011

34. Stribbling SM, Ryan AJ. The cell-line-derived subcutaneous tumor model in preclinical cancer research. *Nat Protoc*. 2022;17(9):2108-2128. doi: 10.1038/s41596-022-00709-3

35. Bylicky MA, Shankavaram U, Aryankalayil MJ, *et al*. Multiomic-Based Molecular Landscape of FaDu Xenograft Tumors in Mice after a Combinatorial Treatment with Radiation and an HSP90 Inhibitor Identifies Adaptation-Induced Targets of Resistance and Therapeutic Intervention. *Mol Cancer Ther*. 2024;23(4):577-588. doi: 10.1158/1535-7163.Mct-23-0796

36. Fantini V, Bordoni M, Scocozza F, *et al*. Bioink Composition and Printing Parameters for 3D Modeling Neural Tissue. *Cells*. 2019;8(8):830.

37. Batista Napotnik T, Miklavčič D. *In vitro* electroporation detection methods – An overview. *Bioelectrochem*. 2018;120:166-182. doi: 10.1016/j.bioelechem.2017.12.005

38. Ruzgys P, Jakutavičiūtė M, Šatkauskienė I, Čepurnienė K, Šatkauskas S. Effect of electroporation medium conductivity on exogenous molecule transfer to cells *in vitro*. *Sci Rep*. 2019;9(1):1436. doi: 10.1038/s41598-018-38287-8

39. Dermol J, Miklavčič D. Predicting electroporation of cells in an inhomogeneous electric field based on mathematical modeling and experimental CHO-cell permeabilization to propidium iodide determination. *Bioelectrochem*. 2014;100:52-61. doi: 10.1016/j.bioelechem.2014.03.011

40. Batista Napotnik T, Polajžer T, Miklavčič D. Cell death due to electroporation – A review. *Bioelectrochem*. 2021;141:107871. doi: 10.1016/j.bioelechem.2021.107871

41. Marazzi D, Carotenuto F, Trovalusci F, Caruccio P, Nardo P. Mechanisms, Models, and Clinical Applications of Cell Membrane Electroporation. *Int J Transl. Sci*. 2025;2024(4):257-302. doi: 10.13052/ijts2246-8765.2024.041

42. Pisani S, Bertino G, Prina-Mello A, *et al*. Electroporation in Head-and-Neck Cancer: An Innovative Approach with Immunotherapy and Nanotechnology Combination. *Cancers*. 2022;14(21):5363.

43. Sonaye SY, Ertugral EG, Kothapalli CR, Sikder P. Extrusion 3D (Bio)Printing of Alginate-Gelatin-Based Composite Scaffolds for Skeletal Muscle Tissue Engineering. *Mater (Basel)*. 2022;15(22):7945. doi: 10.3390/ma15227945

44. Xiao J, Song Y, Gao R, *et al*. Changes of immune microenvironment in head and neck squamous cell carcinoma in 3D-4-culture compared to 2D-4-culture. *J Transl Med*. 2023;21(1):771. doi: 10.1186/s12967-023-04650-1

45. Friedrich J, Seidel C, Ebner R, Kunz-Schughart LA. Spheroid-based drug screen: considerations and practical approach. *Nature Protocols*. 2009;4(3):309-324. doi: 10.1038/nprot.2008.226

46. Rasouli M. Basic concepts and practical equations on osmolality: Biochemical approach. *Clin Biochem*. 2016;49(12):936-41. doi: 10.1016/j.clinbiochem.2016.06.001

47. Johnson DE, Burtness B, Leemans CR, Lui VWY, Bauman JE, Grandis JR. Head and neck squamous cell carcinoma. *Nat Rev Dis Primers*. 2020;6(1):92. doi: 10.1038/s41572-020-00224-3

48. Lin CJ, Grandis JR, Carey TE, *et al*. Head and neck squamous cell carcinoma cell lines: Established models and rationale for selection. *Head & Neck*. 2007;29(2):163-188. doi: 10.1002/hed.20478

49. Valdembri D, Serini G. The roles of integrins in cancer. *Fac Rev*. 2021;10:45. doi: 10.12703/r/10-45

50. Datta P, Dey M, Ataie Z, Unutmaz D, Ozbolat IT. 3D bioprinting for reconstituting the cancer microenvironment. *npj Precis Oncol*. 2020;4(1):18. doi: 10.1038/s41698-020-0121-2